Proceedings of ASME Turbo Expo 2023
Turbomachinery Technical Conference and Exposition
GT2023
June 26-30, 2023, Boston, Massachusetts

GT2023-102634

NUMERICAL ASSESSMENT OF THE EFFECT OF HYDROGEN ENRICHMENT OF A TECHNICALLY PREMIXED SWIRL-STABILIZED NATURAL GAS FLAME

Leonardo Pachano[1,2,*], Anurag Surapaneni[1], Ambrus Both[1], Holger Ax[3], Niklas Petry[3], Isaac Boxx[3,4], Daniel Mira[1]

[1]Barcelona Supercomputing Center (BSC), Barcelona, Spain
[2]Universitat Politènica de València, Valencia, Spain
[3]Institute of Combustion Technology, German Aerospace Center (DLR), Stuttgart, Germany
[4]Lehrstuhl für Optische Messverfahren für die Energie- und Verfahrenstechnik, Rheinisch-Westfälische Technische Hochschule Aachen, Aachen, Germany

ABSTRACT

High-fidelity large eddy simulations (LES) are conducted for lean natural gas flames with different levels of hydrogen enrichment in a technically premixed swirl-stabilized combustor (PRECCINSTA) operated at atmospheric pressure. The modelling approach relies on tabulation of premixed flamelets and presumed-shape probability density functions (PDF) to account for subgrid turbulence-chemistry interactions. Results are presented for non-reacting and reacting conditions with 0, 40 and 50% hydrogen content in the natural gas. The influence of hydrogen-enrichment is investigated here by combining LES with Raman measurements. The assessment of LES shows good predictions of the flame stabilization mechanism, flow field and flame dynamics as compared to experiments. The natural gas flame develops a self-excited flow oscillation characterized as a precessing vortex core, which is well reproduced by the LES. The lean operation of the burner with natural gas shows a stable M-shape flame that transitions to a V-shape fully attached flame as the main fuel is blended with hydrogen. Raman measurements are compared with LES data to examine the flame structure and burning characteristics. It is concluded that hydrogen addition makes the flame more compact, induces higher reactivity of the fuel-air mixture and leads to a stable V-shape flame fully attached to the burner's nozzle-cone.

Keywords: Hydrogen-enrichment, confined swirl flame, flame topology

1. INTRODUCTION

The use of hydrogen as a substitute for conventional hydrocarbons is an appealing alternative in the path towards the decarbonization of the power sector. The blending of hydrogen with conventional fuels is an interesting solution, as it allows to use existing combustion hardware with minimal changes in infrastructure. However, hydrogen-enrichment of conventional fuels can introduce fundamental changes in the combustion characteristics that influence the stability, emissions or thermoacoustics of the system. A recent review on swirl-stabilised lean-premixed combustors highlighted the uncertainty in operability associated to the addition of hydrogen into the fuel mixture, which can have either positive or detrimental effects on flame stability [1]. For instance, the lean blowout limit of a lab-scale gas turbine combustor operated with methane-hydrogen blends was significantly reduced by increasing the contect of hydrogen, while flashback limits revealed varied trends for different flame shapes [2]. A trade-off between improved blow-off resistance and increased flashback tendency was shown to be part of the blending effects of methane/hydrogen mixtures on commercial premixed burners [3]. The PRECCINSTA burner [4], which is a widely studied gas turbine model combustor with an optically accessible combustion chamber, has also been used to investigate the dynamics of hydrogen-enriched natural gas flames from atmospheric to moderate pressures [5] in the combustion test rig HIPOT at DLR Stuttgart.

The atmospheric version of this combustor [4] has been the subject of numerous investigations, including a broad variety of modelling approaches. Among the different strategies, dynamic formulations of the Thickened Flame Model (TFM) [6, 7], Eulerian Stochastic subgrid probability density function (PDF) approaches [8], Scalar Filtered Mass Density Function (SFMDF) with a lagrangian Monte Carlo scheme [9], and the Direct Quadrature Method of Moments (DQMoM) [10] have been explored in the literature. All of the aforementioned approaches have proven successful in reproducing technically premixed combustion with either methane or natural gas. LES results from tabulated chemistry approaches [11–13], under the assumption of perfectly premixed combustion, have also been shown to correlate well with

*Corresponding author: leonardo.pachano@bsc.es

TABLE 1: SUMMARY OF OPERATING CONDITIONS FOR THE TEST CASES

Case	H_2 [% $vol.$]	P_{comb} [bar]	T_{plen} [K]	$\dot{m}_{air}$ [g/s]	ϕ_g [$-$]	$S_L(\phi_g)$ [cm/s]	$\delta_{th}(\phi_g)$ [mm]
1	No fuel	0.99	585	17.6	0	-	-
2	0	1.06	607	17.6	0.71	70.3	0.40
3	40	1.06	590	17.2	0.69	91.2	0.34
4	50	1.05	590	17.0	0.71	107.1	0.31

experimental observations. More in line with the modelling approach addressed in this work, LES coupled to a multidimensional flamelet database for non-premixed combustion, relying on the tabulation of 1D premixed flame solutions at different equivalence ratios, was able to reproduce the swirl-stabilized flames from the PRECCINSTA burner operated at the atmospheric pressure test rig [14]. The results show good correlation with the experimental data and the correct prediction of the V-shape flame for two different equivalence ratios. Flamelet-based combustion models have been used to study hydrogen-enriched (50% by volume) methane combustion in swirl-stabilized flames. LES of the turbulent non-premixed Sydney flame series [15, 16] highlight the feasibility of flamelet-based combustion models while stressing the need of accurate mixing predictions that otherwise can lead to large discrepancies in the prediction of the temperature field. The flamelet generated manifold (FGM) approach has also been reported to perform well in predicting hydrogen-enriched (33% by volume) methane combustion in a partially premixed gas turbine combustor [17] with the focus placed on NO_x predictions. The work also reported a change in the flame morphology towards a more compact flame with the addition of hydrogen. LES-TFM studies focused on the effect of various degrees of hydrogen enrichment have been reported as well. Addition of 40 and 80% hydrogen (by volume) to methane was shown to favor the attachment of the flame through changes in reactivity and radical concentrations at the flame root in a lean premixed swirl-stabilized burner [18].

Fewer numerical studies have addressed the effect of hydrogen enrichment in the PRECCINSTA burner and most works have been conducted with finite rate chemistry models. Agostinelli et al. [19] employed the dynamic formulation of the TFM (DTFLES) and Analytically Reduced Chemistry (ARC) on the atmospheric test rig. Lean flames fueled with hydrogen-enriched methane with 20 and 50% of hydrogen content were correctly reproduced in terms of flow dynamics and flame topology. The addition of hydrogen was shown to modify the flame shape and the root stabilization position. Shorter flames with hydrogen addition were reported to be the result of increased laminar flame speed. From the same research group, the study was extended to the PRECCINSTA at the HIPOT test rig to investigate hydrogen enrichment effects (40% by volume) at elevated pressure [20].

The main objective of this work is to assess the feasibility of a tabulated chemistry approach based on the flamelet method to predict the flame dynamics and stabilization of hydrogen-enriched flames in the PRECCINSTA burner at the HIPOT test rig. This is, to the best of the authors' knowledge, the first numerical study of this configuration [5] using a tabulated chemistry approach. In addition, the study introduces new Laser Raman spectroscopy measurements that provide outstanding information density on the thermo-chemical flame state.

2. OPERATING CONDITIONS AND EXPERIMENTAL SETUP

The computational cases in this study correspond to the swirl-stabilized flames from the PRECCINSTA burner experimentally investigated at the high pressure optical test rig HIPOT from DLR Stuttgart [5]. From this set of experiments, this work targets cases at atmospheric pressure and various degrees of hydrogen enrichment with operating conditions summarized in Table 1. Case 1 is an inert case with no fuel supplied to the system. The rest of cases are reacting cases operating with lean global equivalence ratios (ϕ_g) fueled with pure natural gas (Case 2) and blends with hydrogen in ratios by volume of 40% (Case 3) and 50% (Case 4). Particle Image Velocimetry (PIV) [5] and Planar Laser-Induced Fluorescence of the hydroxyl radical (OH-PLIF) [20] measurements have been used to assess the prediction of the flow field and flame topology, respectively. In this work, the experimental data set is extended by laser Raman measurements on Case 2 and Case 3 providing valuable insights into the thermo-chemical states of the flames.

The burner is characterized by the supply of pre-heated air from a plenum through a 12-vane swirler over a cone-shaped nozzle with exit diameter $D_0 = 27.85\ mm$. The combustor operates under technically premixed conditions with the fuel injected at the swirler's vanes through small orifices of diameter $d = 1\ mm$. The combustion chamber has a square section of $80 \times 80\ mm^2$ and a total length of 200 mm. The exit of the combustion chamber is coupled to a contracting duct of inner diameter $D_e = 18\ mm$.

2.1 Laser Raman spectroscopy

Laser Raman scattering was used for one-dimensional quantitative measurements of the major species concentrations (O_2, H_2, H_2O, CO_2, CO, CH_4, N_2), mixture fraction and temperature. A custom-made long-pulse laser was used (Amplitude Continuum, model Agilite 5-6-12) for the excitation of the virtual state of the respective species. The temporal pulse shaping is based on a user-defined modulation and subsequent amplification of a fraction of a continuous wave (CW) laser. The amplification is achieved by four flash lamp pumped Nd:YAG amplifier stages at a repetition rate of 10 Hz. The pulse duration was set to $\tau_{pulse} = 2\ \mu s$, the laser beam was frequency doubled to a wavelength of $\lambda = 532\ nm$ with a remaining pulse energy of around $E_{pulse} = 1\ J$/pulse at the measurement location. The temporal energy distribution of the laser pulse resembled a nearly rectangular shape.

As can be seen in Figure 1, the beam is redirected via a periscope before being expanded via a Galelei telescope. By

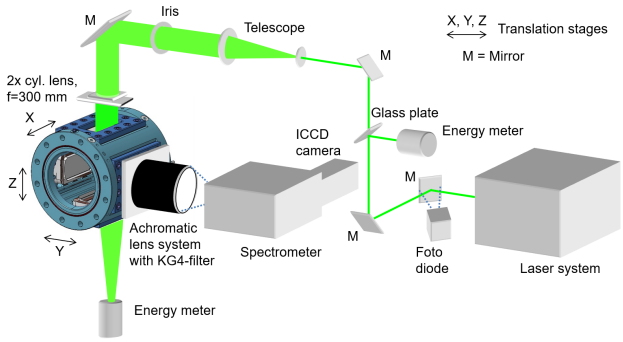

FIGURE 1: LASER RAMAN SPECTROSCOPY SET UP.

means of two cylindrical lenses, the beam is focused to a "blurred" focus on the center of the combustion chamber in order to reduce the laser intensity on the inner window surfaces. The laser energy is measured via two pyroelectric detectors (Gentec-EO, model QE50LP-H-MB-QED-D0), one in front of the combustion chamber and one behind. The Raman scattering from a section along the laser beam with a length of 11.4 mm was focused by an apochromatic lens system (f = 230 mm, aperture = 150 mm) and directed into the entrance slit of a spectrograph (Acton Research SpectraPro 300i; f = 300 mm; f/4.2, 490.4 lines/mm, slit: 1 $mm \times 14$ mm). The elastic scattered light and stray light were reduced with a notch filter (λ = 532 nm) positioned in front of the entrance slit. An intensified CCD (Princeton Instruments PI-Max; 1340 × 1300 pixel, 16 Bit/pixel) was mounted at the exit aperture of the spectrograph. With a hardware binning of the pixels to superpixels, the noise could be reduced significantly. The final digital resolution of a single shot image was 28 × 268 superpixels corresponding to 28 linear measurement volumes, each with a spatial resolution of 0.4 mm in beam direction and a diameter of 0.5 mm given by the laser beam waist and a spectral resolution of 0.61 nm. Though measurements were taken at over 100 different positions within the central horizontal plane (xy) of the combustion chamber, results are only shown for some selected locations in this work. Regarding the z direction, the results presented in this work display only the results from three central measurement volumes out of the 28 as a compromise between spatial resolution (3 × 0.4 mm in z direction with a diameter of 0.5 mm in x and y) and statistic significance. For each measurement position, 300 single shot spectra were recorded.

Evaluation. The data reduction and evaluation of the recorded spectra is based on a calibration data set that was experimentally obtained before the actual flame measurements. The temperature dependent calibration coefficients of the Raman signals of each measured species as well as cross talk effects (spectral overlapping of signals from different species) were determined in a wide temperature range at atmospheric pressure. An electrical gas heater was used for the temperature range from ambient to around 800 K on air, CO, CO_2, CH_4 and H_2. Well defined laminar methane/air and hydrogen/air flames were used at different equivalence ratios and mass flows for the larger temperature range of 1200–2100 K [21, 22]. The calibration measurements were performed in the actual environment of the test rig in order to account for the spectral sensitivity of the spectrograph and the camera and for local optical effects like magnification and imaging of the Raman scattered light. Each spectrum is corrected for background luminosity and normalized regarding pressure, intensifier gain and laser pulse energy. A more detailed description of the calibration procedure is given in [23].

The evaluation of the species concentrations is carried out via an iterative algorithm [24, 25]. Using the temperature-dependent calibration coefficients determined beforehand, the species number densities are calculated and subsequently the molar fractions and the temperature by means of the ideal gas law and the measured pressure within the combustion chamber. Each single shot spectrum is corrected for background luminosity, the intensifier gain, the laser pulse energy and a scaling factor that was determined on a daily base by recording reference spectra of air at known conditions referring to pressure and temperature. The mixture fraction is calculated using the definition proposed by Bilger [26]. The advantage of this definition is the independence of the calculated mixture fraction from preferential diffusion which is a major aspect in hydrogen-doped natural gas flames.

The evaluation of the recorded Raman spectra is carried out on a single shot base. This enables a statistical evaluation of the 300 single shots taken at each position in terms of Reynolds averaged mean values and the root mean square (RMS) as a measure for the fluctuations of the quantities. A comprehensive determination of the accuracy would have to be done for each species and measurement individually which is out of the scope of this work. However, the general accuracy can representatively be assessed by an error treatment of the stable calibration flames. Taking the uncertainties of laser pulse energy (2%), pressure (0.5%), fluctuations of the mass flow controllers (2%), temperature (3%), spectral cross talk and signal intensity fluctuations into account, the relative uncertainties can be calculated by propagation of errors to 5.5% for N_2, H_2O and CO_2, 13.3% for O_2, 7.2% for H_2 and 3.4% for the temperature. The species concentrations in the post flame region of a lean flat CH4/air flame at atmospheric pressure are in fact typically reproduced with an accuracy of around 2% for N_2, 7% for H_2O, 8% for CO_2, 14% for O_2 and 6% for the temperature and the mixture fraction. However, systematic uncertainties due to shifts in alignment or signal correction might additionally impair the accuracy.

3. MODELLING APPROACH

The governing equations for chemically reactive flows in the low-Mach number limit using LES are considered in this work, while a flamelet-based turbulent combustion model is used to describe the chemical states. This modelling framework has been developed in the code Alya from BSC [27], which employs a low-dissipation conservative finite element scheme for low-Mach reacting flows [28]. In this formulation, stabilization is only introduced for the continuity equation through a non-incremental fractional-step approach modified for variable density flows. As for time integration, a third order Runge-Kutta scheme is used for momentum and scalars. The computational domain, depicted in Figure 2, comprises the full geometry [5] with inlet air plenum, swirler, nozzle-cone, chamber, exit contracting duct and an outlet reservoir. Simulations are conducted on a hybrid mesh for which the total count of degrees of freedom is around 68 million. At the

swirler, nozzle-cone and the near field of the flame the resolution is 0.25 mm. The time step is defined by the stability condition with CFL = 0.95. This resolution leads to ratios of Kolmogorov scale respect to mesh resolution $\eta/\Delta \approx 100$ and in terms of flame thickness $\delta_{th}/\Delta \approx 5$. Boundary conditions comprise iso-thermal walls, standard convective out-flow, and steady in-flow for the air inlet. Synthetic turbulence is introduced in the fuel inlet following [29] to better describe the mixing process.

The Navier-Stokes equations in the low-Mach number limit assuming unity Lewis number, are described by the Favre-filtered governing equations Eq. (1), Eq. (2), and Eq. (3) for continuity, momentum, and enthalpy, respectively:

$$\frac{\partial \bar{\rho}}{\partial t} + \nabla \cdot (\bar{\rho}\widetilde{\mathbf{u}}) = 0, \tag{1}$$

$$\frac{\partial (\bar{\rho}\widetilde{\mathbf{u}})}{\partial t} + \nabla \cdot (\bar{\rho}\widetilde{\mathbf{u}}\widetilde{\mathbf{u}}) = -\nabla \cdot \bar{\tau}_M - \nabla \bar{p} + \nabla \cdot \tau (\widetilde{\mathbf{u}}), \tag{2}$$

$$\frac{\partial \left(\bar{\rho}\widetilde{h}\right)}{\partial t} + \nabla \cdot \left(\bar{\rho}\widetilde{\mathbf{u}}\widetilde{h}\right) = -\nabla \cdot \bar{\tau}_h + \nabla \cdot \left(\bar{\rho}\widetilde{D}\nabla\widetilde{h}\right). \tag{3}$$

In this notation, filtered quantities accentuated with a bar denote Reynolds-filtering, while Favre-filtering is expressed by a tilde, being $\bar{\rho}$, $\widetilde{\mathbf{u}}$, $\bar{p}$, $\widetilde{h}$, and $\widetilde{D}$ the filtered density, velocity, pressure, sum of sensible and chemical enthalpy, and diffusivity, respectively. In Eq. (2), $\bar{\tau}_M$ accounts for the unresolved momentum flux and, likewise, in Eq. (3), $\bar{\tau}_h$ accounts for the unresolved enthalpy flux. Heating due to viscous forces is neglected in the enthalpy equation and the unresolved heat flux is modeled using a gradient diffusion approach [30]. The unresolved momentum transport is modelled using the Boussinesq approximation [31] and the eddy viscosity (ν_t) is estimated by Vreman's model [32] using $c_k = 0.1$ as in previous works [28, 33].

The combustion process is described by the tabulation of premixed flamelets. Based on the flamelet method, solutions of 1D premixed laminar flames [34] are computed at different equivalence ratios for various enthalpy levels. Enthalpy variations are introduced to account for heat losses by using burner-stabilized premixed flames [14]. A low-dimensional manifold with three control variables, namely the mixture fraction (Z), the progress variable (Y_c) and the normalized enthalpy (i), is built from these flamelets to recover the laminar flame structure. The mixture fraction is defined following Bilger's formula [26], while the progress variable is defined as a linear combination of certain species mass fractions following $Y_c = Y_{CO_2}/W_{CO_2} + Y_{CO}/W_{CO} + Y_{H_2O}/W_{H_2O}$ [35], where W_k denotes the molecular weight of species k. The normalized enthalpy is defined by $i = (h - h_{min})/(h_{max} - h_{min})$, where h_{min} and h_{max} correspond to the minimum and maximum enthalpy levels of the flamelet for a given mixture fraction.

A presumed-shape PDF is used to take into consideration subgrid turbulence-chemistry interactions. This closure needs to account for fluctuations in composition as this can have a strong influence on the flame stability and flame dynamics [19, 33]. Considering the requirements in data storage for multidimensional databases with composition variations and heat loss, a β-function is used to describe the statistical distribution of Z, while δ-functions are used for both Y_c and i. The correct parametrization of the mixture fraction through the β-function requires the variance of mixture fraction Z_v, given by $Z_v = \widetilde{Z^2} - \widetilde{Z}\widetilde{Z}$. To simplify the tabulation, a scaled progress variable C is defined to access the database so any quantity $\widetilde{\psi}$ from the manifold can be recovered by:

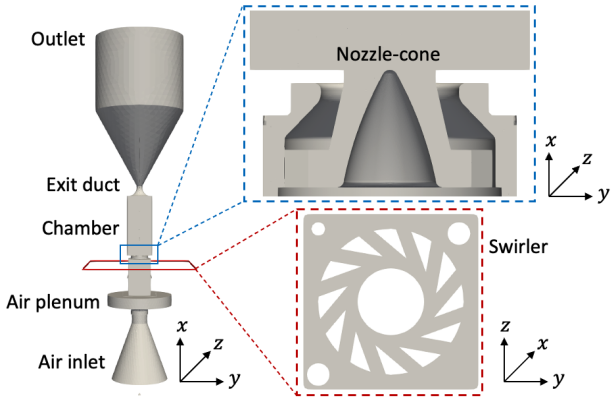

FIGURE 2: LES COMPUTATIONAL DOMAIN.

$$\widetilde{\psi}(C, Z, i) = \int_0^1 \int_0^1 \int_0^1 \psi(C, Z, i)\, \widetilde{P}(C, Z, i)\, dC dZ di, \tag{4}$$

where the joint-PDF is approximated as $\widetilde{P}(C, Z, i) \approx \widetilde{P}_C \widetilde{P}_Z \widetilde{P}_i$ assuming statistical independence [36].

Finally, the governing equations for the three control variables follow Eq. (5), Eq. (6), and Eq. (7):

$$\frac{\partial \left(\bar{\rho}\widetilde{Z}\right)}{\partial t} + \nabla \cdot \left(\bar{\rho}\widetilde{\mathbf{u}}\widetilde{Z}\right) = -\nabla \cdot \bar{\tau}_Z + \nabla \cdot \left(\bar{\rho}\widetilde{D}\nabla\widetilde{Z}\right), \tag{5}$$

$$\frac{\partial \left(\bar{\rho}\widetilde{Y}_c\right)}{\partial t} + \nabla \cdot \left(\bar{\rho}\widetilde{\mathbf{u}}\widetilde{Y}_c\right) = -\nabla \cdot \bar{\tau}_{Y_c} + \nabla \cdot \left(\bar{\rho}\widetilde{D}\nabla\widetilde{Y}_c\right) + \bar{\omega}_{Y_c}, \tag{6}$$

$$\frac{\partial (\bar{\rho}Z_v)}{\partial t} + \nabla \cdot (\bar{\rho}\widetilde{\mathbf{u}}Z_v) = -\nabla \cdot \bar{\tau}_{Z_v} + \nabla \cdot \left(\bar{\rho}\widetilde{D}\nabla Z_v\right) - 2\bar{\tau}_Z \cdot \nabla\widetilde{Z} - 2\bar{S}_{XZ}. \tag{7}$$

The unresolved scalar transport $\bar{\tau}_Z$ in Eq. (5) and $\bar{\tau}_{Y_c}$ in Eq. (6) come from the filtering operation and are closed by a gradient diffusion approach [30]. In Eq. (6), $\bar{\omega}_{Y_c}$ is the filtered source term of Y_c and lastly, $\bar{S}_{XZ}$ in Eq. (7) is the unresolved contribution to the scalar dissipation rate for Z. This term is modeled, under the assumption of linear relaxation at subgrid level [37], according to $\bar{S}_{XZ} = \bar{\rho} Z_v \nu_t / \Delta^2$, where Δ is the filter length associated to the mesh.

The manifold is discretized with 101 points for $\widetilde{Z}$, 101 points for $\widetilde{C}$, 11 points for Z_v, and 16 points for i. The set of reactions and species describing fuel oxidation comes from the GRI-Mech 3.0 [38], which comprises 325 reactions and 53 species.

4. RESULTS AND DISCUSSION

4.1 Mean flow field

Quantitative validation of LES results is conducted by comparing the velocity field with PIV data from the experiments by Chterev and Boxx [5]. Axial velocity profiles are extracted at

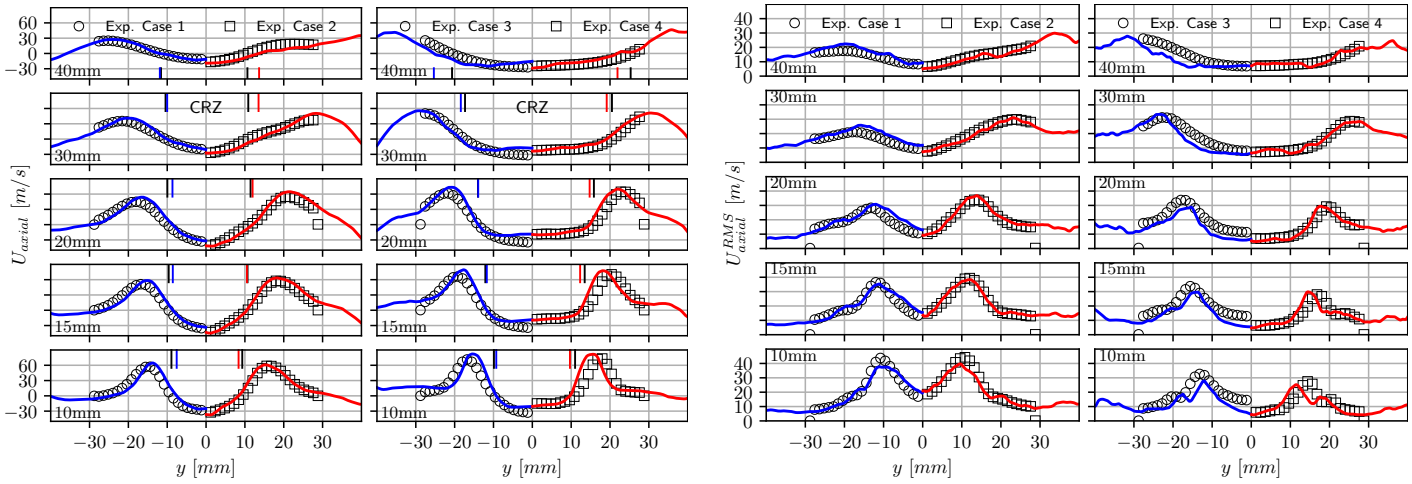

(a) Mean axial velocity profiles.

(b) RMS of axial velocity profiles.

FIGURE 3: VELOCITY PROFILES ACROSS THE CHAMBER.

different locations across the combustion chamber. Mean and RMS profiles of axial velocity are presented in Figure 3 for the four test cases given in Table 1. LES predictions are plotted with a solid line, while experimental measurements use markers. The vertical lines mark the location of the central recirculation zone (CRZ) from the LES (blue and red lines) and the measurements (black line).

Comparison of results for Case 1 and Case 2 in Figure 3a (left) shows a widening of the CRZ with slightly higher peak velocity values at the chamber's axis when going from inert to reacting conditions. The same effect can also be distinguished at the shear layers. Besides mean values, results in Figure 3b (left) also show the comparisons in terms of fluctuations of the axial velocity. Good correlation between LES and experiments is observed for both mean and RMS values. The same trend is also observed for the hydrogen-enriched conditions, Case 3 and Case 4, for which a good correlation with the experiments can be seen. By adding hydrogen to natural gas, further widening of the CRZ is observed with a slight increase in the peak velocity of the jets. The agreement for Case 3 is limited to some extent with numerical profiles exhibiting a flatter shape at the CRZ and with lower fluctuations, see Figure 3a (right) and Figure 3b (right), but overall the correlation is rather good. In contrast, results for Case 4 also follow closely the experimental PIV profiles for both mean and RMS, as previously shown for Case 1 and Case 2.

Results along the chamber's axis are consistent with the observations from radial profiles. The different plots in Figure 4 indicate good performance of the modelling approach in predicting the mean and RMS of the axial velocity for all reacting and non-reacting conditions. The stabilization of the flame (further discussed in Sect. 4.2) plays an important role in the flow field. Simulations for the hydrogen-enriched cases predict stable V-shape flames fully attached to the nozzle-cone. While this is also the case for Case 4 in the experimental work, Case 3 exhibited a bi-stable V-shape in which the flame was mainly but intermittently attached to the nozzle-cone. The good correlation between mea-

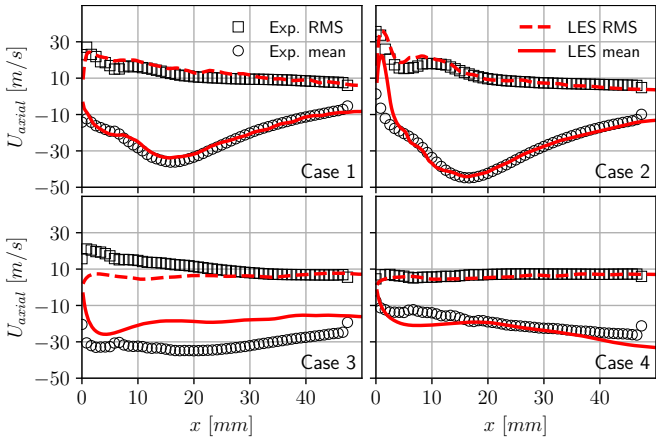

FIGURE 4: VELOCITY PROFILES ALONG THE CHAMBER'S AXIS.

surements and predictions for the V-shape flame at 50% hydrogen addition is in line with the predictions of the mean and RMS of the axial velocity field. On the opposite side, the prediction of a V-shape fully attached flame for the 40% hydrogen-enriched case, as opposed to the measured bi-stable V-shape flame, causes the discrepancies observed between the numerical and experimental results.

Predictions of the mean flow field show that the flow solver can reproduce the hydrodynamics of the swirl-stabilized model combustor under non-reacting and reacting conditions. For the latter, the proposed tabulated approach reproduces the trends observed when adding hydrogen to natural gas characterized by a widening of the CRZ along with lower velocities at this location and higher velocities at the jets. In addition to the validation of the mean flow field, the assessment of the flame dynamics is presented in Sect. 4.1 before evaluating the stabilization of the flame for the different levels of hydrogen enrichment in Sect. 4.2.

Flame dynamics. One of the most distinct phenomena of the studied conditions is the presence of a precessing vortex core

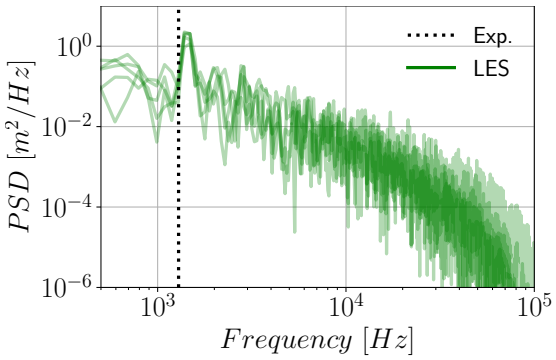

FIGURE 5: AXIAL VELOCITY PSD FOR CASE 2.

(PVC) for the M-shape flame from Case 2. This self-excited flow oscillation was reported by the experiments [5] and it manifests with a characteristic frequency, denoted by f_{PVC} herein. In order to characterize the PVC from the LES, the power spectral density (PSD) of the axial component of the flow velocity is computed from a modified periodogram with a 50% overlap. The green lines in Figure 5 correspond to the PSD from data collected along the inner shear layer (ISL), while the vertical dashed line marks the f_{PVC} measured experimentally. The characteristic frequency of the PVC from the LES (distinct peak value from the PSD) is predicted with less than 7% error, at a value of $f_{PVC} = 1385\ Hz$. The V-shape topology, distinctive of the hydrogen-enriched conditions, has been reported to weaken the intensity of the PVC [5]. In line with this observation, no distinct peak values were found from the PSD of the axial velocity from Case 3 and Case 4 in agreement with the experimental data.

4.2 Flame stabilization

In this section, an analysis of unsteady effects introduced by hydrogen enrichment is presented. Experimental measurements reported by Chterev and Boxx [5] show a transition in the flame stabilization mechanism by increasing the hydrogen content in the fuel. Figure 6 shows instantaneous LES results of temperature and axial velocity depicting the characteristic M- and V-shape flames. In the pure natural gas flame (Case 2), the flame stabilizes with an M-shape detached from the nozzle-cone. This M-shape flame transitions to a V-shape flame fully attached to the nozzle-cone when the fuel is enriched with hydrogen (Case 3 and Case 4). Experimentally, the 40% hydrogen condition exhibits a bi-stable V-shape topology with the flame mainly but intermittently attached to the nozzle-cone, while the 50% hydrogen condition is described as a fully attached V-shape flame. These two complex conditions require appropriate modelling and numerical strategies that can reproduce such transient conditions. Stable operating points with M- and V-shape flames (Case 2 and Case 4) are reproduced well with the proposed modelling approach. The location of the shear layers is well predicted as seen in the iso-contour of zero mean axial velocity in Figure 7. This figure also shows the normalized time-averaged OH mass fraction field and compares it with the normalized PLIF-OH measurements. Case 2 (Figure 7 left) shows an M-shape flame that stabilizes with a certain lift-off (around P1). Case 4 (Figure 7 right) is also well predicted with a strong inner layer and weak outer layer. However, some discrepancies appear for Case 3, see middle plot in Figure 7. This case is experimentally found to be bi-stable, with the flame oscillating between the two stable solutions, leading mainly to a V-shape flame and occasionally to an M-shape flame. The proposed modelling approach was not able to reproduce this transitional state, at least at the same equivalence ratio found in the experiment. Nevertheless, the present LES was able to reproduce the global burning characteristics for both stable solutions fairly well. Numerical and experimental results evidence the transition from the M-shape in Case 2 (Figure 7 left) to V-shape in Case 3 and Case 4 (Figure 7 middle and right).

Temperature and equivalence ratio results are retrieved at two locations 8 mm downstream from the tip of the nozzle-cone. These are labeled as P1 and P2 and are radially located at the center of the chamber (P1) and at $y = 15\ mm$ (P2). Figure 8 and Figure 9 show scatter plots from the thermo-chemical states given by the LES and measured by laser Raman spectroscopy. LES predictions show the sensitivity of results to mesh resolution and fuel-air mixing from two inflow conditions for the fuel. Results labeled "T0.25" are baseline results with the modelling approach from Section 3 with the mesh resolution of 0.25 mm and with synthetic turbulence. Results "T0.4" correspond to cases with a coarser mesh resolution of 0.4 mm, while results "L0.4" come from cases with the same mesh but without synthetic turbulence.

Overall, the scatter plots from the LES exhibit a good correlation with the Raman data in terms of flame structure for the two cases. At the jet (location P2), most points come from fresh gases, though some scatter can be distinguished with intermediate and high temperatures. For Case 2, some discrepancies between the LES and the experiments can be observed in the CRZ (P1). The single-shot experiments at P1 show more scatter around the temperature of fresh gases with fewer points at intermediate and high temperatures compared to LES results. While the thermo-chemical states measured experimentally are centered around ϕ_g, the LES predicts a richer and more reactive mixture. The tendency to predict richer mixtures (relative to ϕ_g) is also noticeable at P1 for Case 3. High-temperature gases at location P1 are richer than those of the experiment that reveal temperature fluctuations at intermediate temperatures. For all three cases, peak temperatures are in line with temperature at equilibrium from the flamelet solutions, but at richer conditions than ϕ_g. Experimentally determined temperatures beyond the adiabatic value are due to the inherent statistical scattering of the Raman process and to some extend, due to the reduced signal to noise ratio at lower density that impair the accuracy. The measured mean temperature of the fully burned samples is lower than the adiabatic flame temperature, presumably due to heat loss by the combustion chamber walls and the nozzle tip.

Discrepancies in the predicted range of equivalence ratio is attributed to limitations in the prediction of the jet in cross-flow mixing process within the swirler. It has been reported that accurate prediction of the jet in cross-flow in canonical configurations requires high mesh resolution and accounting for the turbulence of the fuel jet [39, 40]. The computational cost of these requirements is prohibitive for the case under study with 12 injectors of 1 mm diameter. Results "T0.4" and "T0.25" show that while changing the resolution from 0.4 mm to 0.25 mm the range of

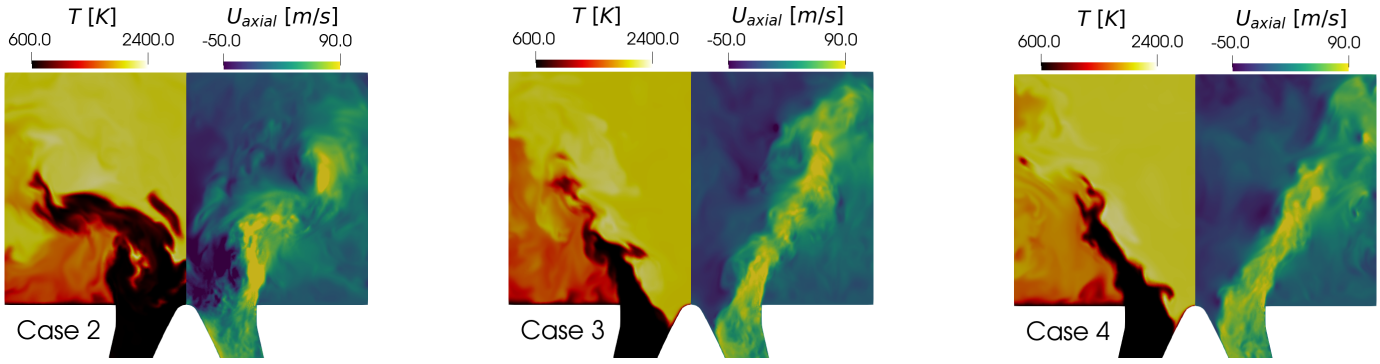

FIGURE 6: LES INSTANTANEOUS RESULTS. AT EACH PANEL TEMPERATURE (LEFT) AND AXIAL VELOCITY (RIGHT).

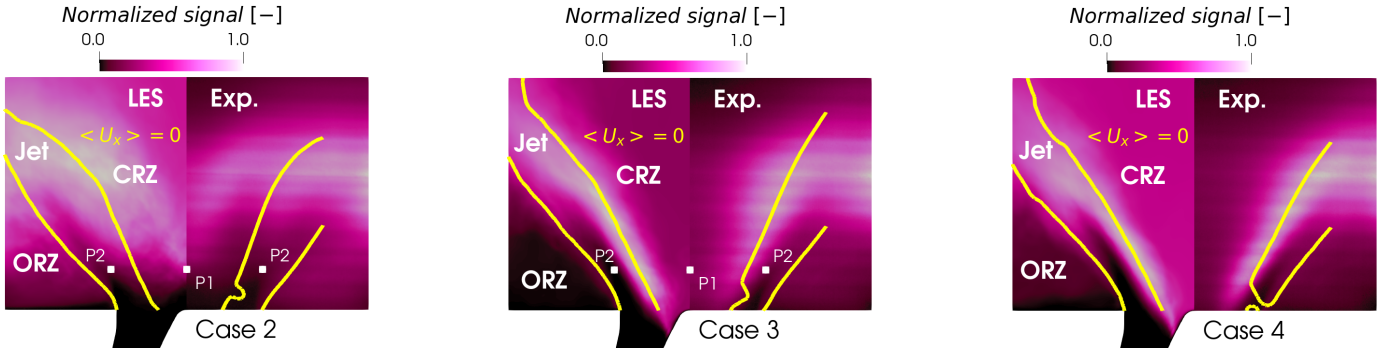

FIGURE 7: FLAME TOPOLOGY. AT EACH PANEL NORMALIZED MEAN Y_{OH} (LEFT) AND PLIF-OH (RIGHT).

mixtures is slightly shifted towards leaner mixtures. This is also the case for "L0.4" and "T0.4" which show that improving the mixing prediction (accounting for a transient inflow condition with synthetic turbulence in "T0.4" as compared to the steady condition in "L0.4") also improves the mixing process that eventually affects the prediction of extinction with states slightly below the temperature at equilibrium (most noticeably at P1).

The topology of the M- and V-shape flames is further assessed in Figure 10 by comparing the prediction of the mean temperature, equivalence ratio and mass fractions of methane and water vapour with laser Raman spectroscopy measurements conducted at 13.5 *mm* downstream from the nozzle tip. Predicted mean values do not change for the three setups described for Figure 8 and Figure 9. Hence, Figure 10 only show results for the LES approach proposed in Section 3. Figure 10 (left) shows higher temperature values compared to measurements. While the flow field is well predicted for Case 2 with an M-shape flame, the proposed tabulated chemistry approach tends to slightly underestimate the flame lift-off, see Figure 7. The comparison with the Raman measurements confirms that the flame stabilizes closer to the nozzle tip in comparison to the experiment. The measured temperatures show intermediate mean temperatures and fluctuations. The measurement location is therefore in a region with strong turbulent mixing of fresh gas with hot burned gas resulting in high-temperature fluctuations. LES results for mean values of temperature and source term of the progress variable conditioned to equivalence ratio support this observation, but are not included for the sake of brevity. The profile of equivalence ratio also shows that, in general, the mixture from the LES is richer than the global equivalence ratio of 0.71 as observed in the scatter plot from Figure 8. Predicted values of ϕ closer to stoichiometry go in line with higher temperatures and the stabilization of the flame closer to the nozzle tip due to a more reactive mixture. This observation is also supported by the prediction of lower methane mass fractions and higher water vapour mass fractions compared to measured values. With the M-shape flame stabilized closer to the nozzle tip, less fuel and more products are expected. Predictions for the hydrogen-enriched condition in Figure 10 (right) are in good agreement with measurements as seen for the qualitative comparison of the flame shape, see middle plot in Figure 7. The measured temperatures show much less fluctuations in the central region compared to Case 2, with temperature values of fully burned gases. This shows that the flame is mainly attached to the nozzle or is at least not highly lifted when detached. The dip of the temperature values around the center is consistent with a lower equivalence ratio at this location, and losses by the nozzle tip might additionally reduce the temperature. Higher temperature values predicted within the CRZ can be linked to slightly richer equivalence ratio compared to ϕ_g. As a consequence of an overall richer mixture in the LES, predictions of methane and water vapour mass fractions are also slightly below and above the measured value, respectively.

Lastly, the flame topology is further characterized to examine the impact of hydrogen blending. To that end, the turbulent flame

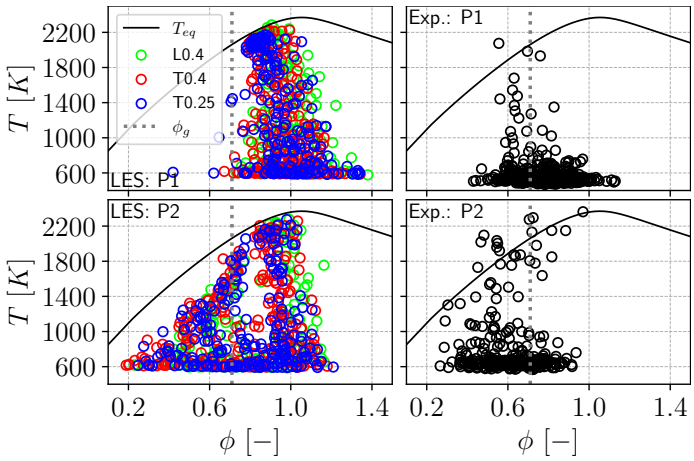

FIGURE 8: THERMO-CHEMICAL STATE AT P1 AND P2 FOR CASE 2.

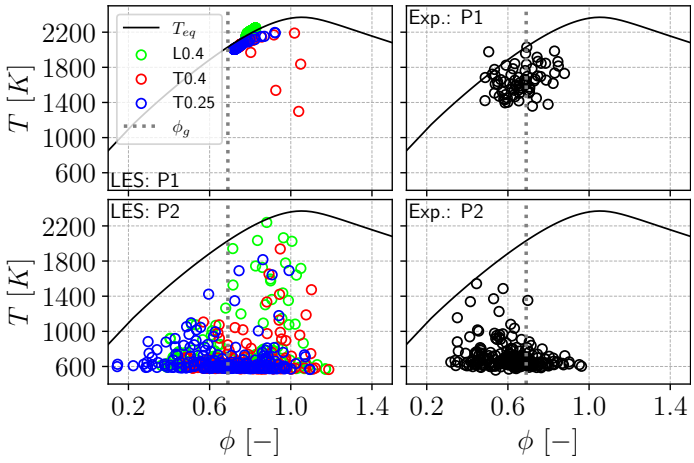

FIGURE 9: THERMO-CHEMICAL STATE AT P1 AND P2 FOR CASE 3.

front surface area (A_T) is computed from the area of the iso-surface of the normalized progress variable $C = 0.5$. Mean values of A_T are found to be 18628.1, 13536.4, and 11676.8 mm^2 with a standard deviation of 1033.9, 471.9, and 497.1 mm^2 for Case 2, Case 3, and Case 4, respectively. Note that smaller values of mean A_T correspond to more compact flames, as seen for the hydrogen-enriched flames, in agreement with the experimental observation. From the standard deviation of A_T, it is also observed that the M-shape flame (Case 2) is characterized by larger fluctuations as opposed to smaller fluctuations for the more stable V-shape flames (Case 3 and Case 4).

5. CONCLUSIONS AND FUTURE WORK

This works presented a numerical investigation of the reacting flow field of a technically premixed swirl-stabilized model combustor using tabulated chemistry in the context of LES. The focus was placed on the assessment of the predicting capabilities of this modelling approach to reproduce the effects of hydrogen blending in natural gas in terms of stabilization mechanism, flame shape and structure.

For the mean flow field, the modelling approach reproduces the main features of the non-reacting condition and trends for the reacting conditions with and without hydrogen content. The

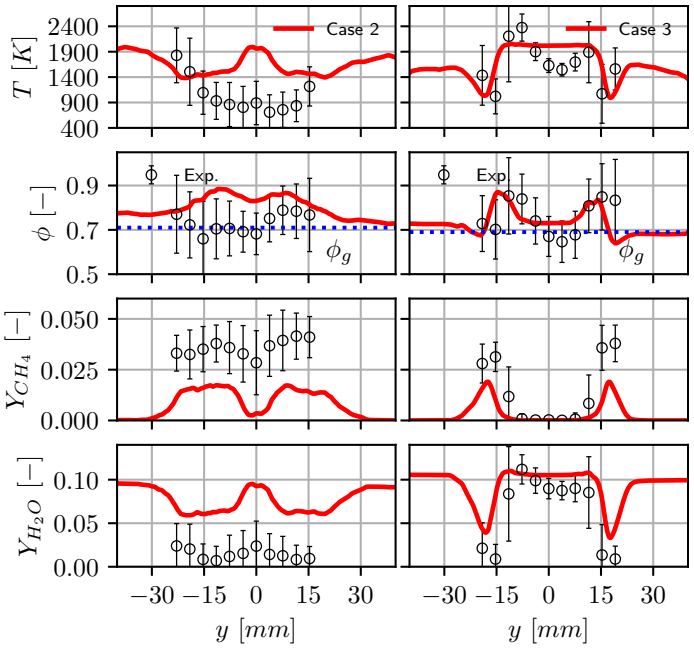

FIGURE 10: MEAN PROFILES OF TEMPERATURE, EQUIVALENCE RATIO, AND MASS FRACTION OF MAJOR SPECIES.

change from non-reacting to reacting conditions introduces a widening of the CRZ. Addition of hydrogen contributes to this widening, while also incresing peak velocities at the jets of incoming fresh gases. Flame dynamics are also well captured by the modelling approach with the characteristic frequency of the PVC for Case 2 in good agreement with measurements. No predominant frequencies were found in the PSD of the axial velocity for Case 3 and Case 4 also in agreement with experiments.

Thermo-chemical states from LES and laser Raman spectroscopy measurements correlate well for Case 2 and Case 3. For the latter, the CRZ is characterized as a zone of fully burned gases at temperatures close to equilibrium in contrast to more fluctuating values recorded experimentally. Accounting for the statistical distribution of the progress variable through a β-function PDF integration (as opposed to the δ-function used in this work) might be used to overcome this shortcoming and could potentially mitigate the lift-off length underprediction observed in Case 2. The influence of turbulence-chemistry interactions on the flame stabilization is left for future work. For the LES, the sensitivity of local results of temperature and equivalence ratio to changes in mesh resolution and prediction of the mixing process has been shown. Increased resolution and improvement of the mixing process of the jet in cross-flow (through a transient inflow condition with synthetic turbulence at the fuel inlets) led to a better correlation with the experimental results. Hydrogen enrichment of natural gas was also shown to enhance mixture reactivity which translates into more compact flames as seen from the predicted turbulent flame front surface area. Results showed higher variations with respect to the mean value for the M-shape flame in comparison to the more stable V-shape flames.

It can be concluded that the proposed tabulated chemistry model is a suitable approach to characterize the influence of hydrogen blending on the flame dynamics and structure in the stud-

ied model combustor with substantial benefits in computational cost reduction with respect to other approaches that require to transport multiple species and integration of the chemical source terms.

ACKNOWLEDGMENTS

This project has received funding from the European Research Council (ERC) under the European Union's Horizon 2020 research and innovation program (grant agreement No. 682383), the Center of Excellence in Combustion project (grant agreement No 952181), and the AHEAD PID2020-118387RB-C33 and ORION TRA2017-89139-C2-2-R projects from the Ministerio de Ciencia e Innovación. Leonardo Pachano acknowledges the Margarita Salas grant from Ministerio de Universidades (Spain) funded by the European Union-Next Generation EU. The authors thankfully acknowledge the computer resources from the RES (IM-2022-2-0003).

REFERENCES

[1] Beita, J., Talibi, M., Sadasivuni, S. and Balachandran, R. "Thermoacoustic Instability Considerations for High Hydrogen Combustion in Lean Premixed Gas Turbine Combustors: A Review." *Hydrogen* Vol. 2 No. 1 (2021): pp. 33–57. DOI 10.3390/hydrogen2010003.

[2] Liu, X., Bertsch, M., Subash, A. A., Yu, S., Szasz, R.-Z., Li, Z., Petersson, P., Bai, X.-S., Aldén, M. and Lörstad, D. "Investigation of Turbulent Premixed Methane/Air and Hydrogen-Enriched Methane/Air Flames in a Laboratory-Scale Gas Turbine Model Combustor." *International Journal of Hydrogen Energy* Vol. 46 No. 24 (2021): pp. 13377–13388. DOI 10.1016/j.ijhydene.2021.01.087.

[3] Aniello, A., Poinsot, T., Selle, L. and Schuller, T. "Hydrogen Substitution of Natural-Gas in Premixed Burners and Implications for Blow-off and Flashback Limits." *International Journal of Hydrogen Energy* Vol. 47 No. 77 (2022): pp. 33067–33081. DOI 10.1016/j.ijhydene.2022.07.066.

[4] Meier, W, Weigand, P, Duan, X and Giezendannerthoben, R. "Detailed Characterization of the Dynamics of Thermoacoustic Pulsations in a Lean Premixed Swirl Flame." *Combustion and Flame* Vol. 150 No. 1-2 (2007): pp. 2–26. DOI 10.1016/j.combustflame.2007.04.002.

[5] Chterev, I. and Boxx, I. "Effect of Hydrogen Enrichment on the Dynamics of a Lean Technically Premixed Elevated Pressure Flame." *Combustion and Flame* Vol. 225 (2021): pp. 149–159. DOI 10.1016/j.combustflame.2020.10.033.

[6] Wang, P., Hashemi, S. M., He, H. and Cheng, K. "Investigation of the Partially Premixed Turbulent Combustion through the PRECCINSTA Burner by Large Eddy Simulation." *Aerospace Science and Technology* Vol. 121 (2022): p. 107336. DOI 10.1016/j.ast.2022.107336.

[7] Agostinelli, P. W., Laera, D., Boxx, I., Gicquel, L. and Poinsot, T. "Impact of Wall Heat Transfer in Large Eddy Simulation of Flame Dynamics in a Swirled Combustion Chamber." *Combustion and Flame* Vol. 234 (2021): p. 111728. DOI 10.1016/j.combustflame.2021.111728.

[8] Fredrich, D., Jones, W. P. and Marquis, A. J. "Thermo-Acoustic Instabilities in the PRECCINSTA Combustor Investigated Using a Compressible LES-pdf Approach." *Flow, Turbulence and Combustion* Vol. 106 No. 4 (2021): pp. 1399–1415. DOI 10.1007/s10494-020-00177-3.

[9] Ansari, N., Strakey, P.A., Goldin, G.M. and Givi, P. "Filtered Density Function Simulation of a Realistic Swirled Combustor." *Proceedings of the Combustion Institute* Vol. 35 No. 2 (2015): pp. 1433–1442. DOI 10.1016/j.proci.2014.05.042.

[10] Emmi, Y., Fiolitakis, A. and Aigner, M. "Numerical Investigation of Swirl-Stabilised Model Gas Turbine Combustor Using DQMoM with LES." *GPPS Chania20*. 2020. Chania, Greece. DOI 10.33737/gpps20-tc-102.

[11] He, H.-K., Wang, P., Xu, L., Xu, Q., Jiang, L.-S. and Shrotriya, P. "Large Eddy Simulation of Lean Premixed Swirling Flames via Dynamically Thickened Flame Model Coupling with the REDIM Chemistry Table." *Combustion, Explosion, and Shock Waves* Vol. 56 No. 6 (2020): pp. 634–647. DOI 10.1134/S0010508220060039.

[12] Wang, P., Fröhlich, J., Maas, U., He, Z.-x. and Wang, C.-j. "A Detailed Comparison of Two Sub-Grid Scale Combustion Models via Large Eddy Simulation of the PRECCINSTA Gas Turbine Model Combustor." *Combustion and Flame* Vol. 164 (2016): pp. 329–345. DOI 10.1016/j.combustflame.2015.11.031.

[13] Wang, P., Platova, N.A., Fröhlich, J. and Maas, U. "Large Eddy Simulation of the PRECCINSTA Burner." *International Journal of Heat and Mass Transfer* Vol. 70 (2014): pp. 486–495. DOI 10.1016/j.ijheatmasstransfer.2013.11.025.

[14] Gövert, S., Mira, D., Kok, J. B. W., Vázquez, M. and Houzeaux, G. "The Effect of Partial Premixing and Heat Loss on the Reacting Flow Field Prediction of a Swirl Stabilized Gas Turbine Model Combustor." *Flow, Turbulence and Combustion* Vol. 100 No. 2 (2018): pp. 503–534. DOI 10.1007/s10494-017-9848-4.

[15] Kempf, A., Malalasekera, W., Ranga-Dinesh, K. K. J. and Stein, O. "Large Eddy Simulations of Swirling Non-premixed Flames With Flamelet Models: A Comparison of Numerical Methods." *Flow, Turbulence and Combustion* Vol. 81 No. 4 (2008): pp. 523–561. DOI 10.1007/s10494-008-9147-1.

[16] Ihme, M., Schmitt, C. and Pitsch, H. "Optimal Artificial Neural Networks and Tabulation Methods for Chemistry Representation in LES of a Bluff-Body Swirl-Stabilized Flame." *Proceedings of the Combustion Institute* Vol. 32 No. 1 (2009): pp. 1527–1535. DOI 10.1016/j.proci.2008.06.100.

[17] Meloni, R., Nassini, P.C. and Andreini, A. "Model Development for the Simulation of the Hydrogen Addition Effect onto the NOx Emission of an Industrial Combustor." *Fuel* Vol. 328 (2022): p. 125278. DOI 10.1016/j.fuel.2022.125278.

[18] Guo, S., Wang, J., Zhang, W., Zhang, M. and Huang, Z. "Effect of Hydrogen Enrichment on Swirl/Bluff-Body Lean Premixed Flame Stabilization." *International Journal of Hydrogen Energy* Vol. 45 No. 18 (2020): pp. 10906–10919. DOI 10.1016/j.ijhydene.2020.02.020.

[19] Agostinelli, P.W., Laera, D., Chterev, I., Boxx, I., Gicquel, L. and Poinsot, T. "On the Impact of H_2-Enrichment on Flame Structure and Combustion Dynamics of a Lean Partially-Premixed Turbulent Swirling Flame." *Combustion and Flame* Vol. 241 (2022): p. 112120. DOI 10.1016/j.combustflame.2022.112120.

[20] Agostinelli, P. W., Laera, D., Chterev, I., Boxx, I., Gicquel, L. and Poinsot, T. "Large Eddy Simulations of Mean Pressure and H 2 Addition Effects on the Stabilization and Dynamics of a Partially-Premixed Swirled-Stabilized Methane Flame." *Combustion and Flame* Vol. 249 (2023): p. 112592. DOI 10.1016/j.combustflame.2022.112592.

[21] Weigand, P., Lückerath, R. and Meier, W. "Documentation of Flat Premixed Laminar CH_4/Air Standard Flames: Temperatures and Species Concentrations." *http://www.dlr.de/vt/datenarchiv* .

[22] Prucker, S., Meier, Wolfgang and Stricker, Winfried. "A Flat Flame Burner as Calibration Source for Combustion Research: Temperatures and Species Concentrations of Premixed H_2/Air Flames." *Review of Scientific Instruments* Vol. 65 No. 9 (1994): pp. 2908–2911. DOI 10.1063/1.1144637.

[23] Ax, H., Kutne, P., Meier, W., König, K., Maas, U., Class, A. and Aigner, M. "Low Pressure Premixed CH_4/Air Flames with Forced Periodic Mixture Fraction Oscillations: Experimental Approach." *Applied Physics B* Vol. 94 (2009): pp. 705–714.

[24] Ax, H., Lammel, O., Lückerath, R. and Severin, M. "High-Momentum Jet Flames at Elevated Pressure, C: Statistical Distribution of Thermochemical States Obtained from Laser-Raman Measurements." *Journal of Engineering for Gas Turbines and Power* Vol. 142 No. 7 (2020). DOI 10.1115/1.4045483.

[25] Stopper, U. "Further Development and Application of Laser Raman Scattering for the Investigation of Industrial Premixed Flames in a High-Pressure Combustion Chamber." Ph.D. Thesis, University of Stuttgart, Stuttgart, Germany. 2014.

[26] Bilger, R.W. "The Structure of Turbulent Nonpremixed Flames." *Symposium (International) on Combustion* Vol. 22 No. 1 (1989): pp. 475–488. DOI 10.1016/S0082-0784(89)80054-2.

[27] Vázquez, M., Houzeaux, G., Koric, S., Artigues, A., Aguado-Sierra, Jazmin, Arís, R., Mira, D., Calmet, H., Cucchietti, F., Owen, H., Taha, A., Burness, E., Cela, J. M. and Valero, M. "Alya: Multiphysics Engineering Simulation toward Exascale." *Journal of Computational Science* Vol. 14 (2016): pp. 15–27. DOI 10.1016/j.jocs.2015.12.007.

[28] Both, A., Lehmkuhl, O., Mira, D. and Ortega, M. "Low-Dissipation Finite Element Strategy for Low Mach Number Reacting Flows." *Computers & Fluids* Vol. 200 (2020): p. 104436. DOI 10.1016/j.compfluid.2020.104436.

[29] Kempf, A., Klein, M. and Janicka, J. "Efficient Generation of Initial- and Inflow-Conditions for Transient Turbulent Flows in Arbitrary Geometries." *Flow, Turbulence and Combustion formerly: Applied Scientific Research* Vol. 74 No. 1 (2005): pp. 67–84. DOI 10.1007/s10494-005-3140-8.

[30] Mira Martinez, D., Jiang, X., Moulinec, C. and Emerson, D.R. "Numerical Assessment of Subgrid Scale Models for Scalar Transport in Large-Eddy Simulations of Hydrogen-Enriched Fuels." *International Journal of Hydrogen Energy* Vol. 39 No. 14 (2014): pp. 7173–7189. DOI 10.1016/j.ijhydene.2014.03.018.

[31] Poinsot, T. and Veynante, D. *Theoretical and Numerical Combustion*. RT Edwards, Inc. (2005).

[32] Vreman, A. W. "An Eddy-Viscosity Subgrid-Scale Model for Turbulent Shear Flow: Algebraic Theory and Applications." *Physics of Fluids* Vol. 16 No. 10 (2004): pp. 3670–3681. DOI 10.1063/1.1785131.

[33] Mira, D., Lehmkuhl, O., Both, A., Stathopoulos, P., Tanneberger, T., Reichel, T. G., Paschereit, C. O., Vázquez, M. and Houzeaux, G. "Numerical Characterization of a Premixed Hydrogen Flame Under Conditions Close to Flashback." *Flow, Turbulence and Combustion* Vol. 104 No. 2-3 (2020): pp. 479–507. DOI 10.1007/s10494-019-00106-z.

[34] van Oijen, J.A., Donini, A., Bastiaans, R.J.M., ten Thije Boonkkamp, J.H.M. and de Goey, L.P.H. "State-of-the-Art in Premixed Combustion Modeling Using Flamelet Generated Manifolds." *Progress in Energy and Combustion Science* Vol. 57 (2016): pp. 30–74. DOI 10.1016/j.pecs.2016.07.001.

[35] Hansinger, M., Ge, Y. and Pfitzner, M. "Deep Residual Networks for Flamelet/Progress Variable Tabulation with Application to a Piloted Flame with Inhomogeneous Inlet." *Combustion Science and Technology* Vol. 194 No. 8 (2022): pp. 1587–1613. DOI 10.1080/00102202.2020.1822826.

[36] Ihme, M. and Pitsch, H. "Prediction of Extinction and Reignition in Nonpremixed Turbulent Flames Using a Flamelet/Progress Variable Model: 2. Application in LES of Sandia Flames D and E." *Combustion and Flame* Vol. 155 No. 1 (2008): pp. 90–107. DOI 10.1016/j.combustflame.2008.04.015.

[37] Domingo, P., Vervisch, L. and Veynante, D. "Large-Eddy Simulation of a Lifted Methane Jet Flame in a Vitiated Coflow." *Combustion and Flame* Vol. 152 No. 3 (2008): pp. 415–432. DOI 10.1016/j.combustflame.2007.09.002.

[38] Smith, G. P., Golden, D. M., Frenklach, M., Moriarty, N. W., Eiteneer, B., Goldenberg, M., Bowman, C. T., Hanson, R. K., Song, S., Gardiner, W. C., Jr., Lissianski, V. V. and Qin, Z. "GRI-Mech 3.0." *http://www.me.berkeley.edu/gri_mech/* .

[39] Walters, DK and Leylek, JH. "A Systematic Computational Methodology Applied to a Three-Dimensional Film-Cooling Flowfield." (1997).

[40] Johnson, P. L. and Kapat, J. S. "Large-Eddy Simulations of a Cylindrical Film Cooling Hole." *Journal of thermophysics and heat transfer* Vol. 27 No. 2 (2013): pp. 255–273.